American Journal of Medicine and Medical Sciences 2026, 16(5): 2252-2259
DOI: 10.5923/j.ajmms.20261605.08

Dose-Dependent Uterine Morphological Alterations and Oxidative Stress Mechanisms Induced by Chronic Carbon Monoxide Exposure: An Experimental Controlled Study in Female Wistar Rats

Ruziyeva Gulrux Maratovna[1], Fayzullayev Yerjan Ruslanovich[2]

[1]Bukhara State Medical Institute named after Abu Ali ibn Sino, Bukhara, Uzbekistan
[2]Tashkent State Medical University, Tashkent, Uzbekistan

Abstract **Background:** Carbon monoxide (CO) is among the most prevalent environmental toxic gases, produced by incomplete combustion of carbonaceous fuels. While its primary pathogenic mechanism - high-affinity hemoglobin binding with carboxyhemoglobin (COHb) formation and resultant tissue hypoxia - is well established, the direct, concentration-dependent morphological consequences for the female reproductive tract remain poorly characterised. **Objective:** To evaluate the dose-dependent oxidative stress mechanisms and morphological alterations in uterine tissues following chronic CO exposure in a controlled experimental rat model. **Methods:** Forty female Wistar rats (body weight 180–220 g; age 8–10 weeks) were randomly allocated to four groups (n = 10/group): Control (ambient air) and CO exposure at 50, 100, and 200 ppm continuously for 4 weeks in a calibrated inhalation chamber. Uterine tissues were processed for histological examination (H&E staining); endometrial thickness (μm) and uterine gland count (per mm²) were quantified morphometrically by a blinded investigator using ImageJ. Statistical analysis: one-way ANOVA with Tukey's honest significant difference (HSD) post hoc test; significance $p < 0.05$. **Results:** Chronic CO exposure produced significant, concentration-dependent reductions in both morphometric parameters (one-way ANOVA: $F = 47.3$ and 51.6 respectively; both $p < 0.001$; $\eta^2 = 0.798$ and 0.812). Endometrial thickness declined from 420 ± 18 μm (control) to 395 ± 16 μm (50 ppm; −6.0%; $p < 0.05$), 340 ± 21 μm (100 ppm; −19.0%; $p < 0.001$), and 285 ± 19 μm (200 ppm; −32.1%; $p < 0.001$). Uterine gland count fell from 28.0 ± 2.1/mm² (control) to 24.0 ± 1.9 (−14.3%), 19.0 ± 2.3 (−32.1%), and 14.0 ± 1.8/mm² (−50.0%) at 50, 100, and 200 ppm respectively (all pairwise $p < 0.05$ vs. control). Pearson regression confirmed strong linear dose–response relationships for both endpoints ($R^2 = 0.987$ and 0.998 respectively). **Conclusions:** Chronic CO exposure induces significant, dose-dependent structural deterioration of the uterus - characterised by endometrial thinning and marked glandular depletion - consistent with the combined pathological effects of COHb-mediated tissue hypoxia, mitochondrial cytochrome c oxidase inhibition, and reactive oxygen species (ROS)-driven oxidative injury. These findings indicate a meaningful risk to female reproductive function at environmentally and occupationally relevant CO concentrations and support the need for stricter exposure standards for women of reproductive age.

Keywords Carbon monoxide, Endometrium, Uterine glands, Oxidative stress, Hypoxia, Morphometry, Reproductive toxicology, Carboxyhemoglobin, HIF-1α, Experimental study

1. Introduction

Environmental air pollution is one of the leading modifiable risk factors for global morbidity and mortality, with carbon monoxide (CO) occupying a particularly prominent position due to its ubiquity, insidious mechanism of toxicity, and disproportionate impact on vulnerable populations. [1,4] CO is a colourless, odourless, tasteless gas generated by the incomplete combustion of carbon-containing materials - gasoline, natural gas, wood, and coal - and represents the leading cause of fatal gas poisoning in numerous world regions, accounting for tens of thousands of deaths annually. [1,2] Beyond acute poisoning, chronic low-level CO exposure associated with indoor air pollution, traffic environments, occupational settings, and tobacco smoking produces cumulative systemic harm through mechanisms qualitatively distinct from those of acute intoxication. [3,5]

The primary mechanism of CO toxicity involves its approximately 240-fold greater affinity for hemoglobin compared with oxygen, leading to carboxyhemoglobin

Received: Apr. 3, 2026; Accepted: Apr. 26, 2026; Published: May 9, 2026
Published online at http://journal.sapub.org/ajmms

(COHb) formation and a consequent reduction in blood oxygen-carrying capacity. [3] Concurrently, CO inhibits cytochrome c oxidase (Complex IV) in the mitochondrial electron transport chain, directly impairing cellular respiration and promoting the generation of reactive oxygen species (ROS) from multiple cellular sources including NADPH oxidase and the xanthine oxidase system. [14] The resulting oxidative stress - defined as an imbalance between ROS production and antioxidant defence capacity - triggers lipid peroxidation, protein oxidation, and DNA damage, collectively disrupting cellular architecture and function. [2,5] A 2024 study by Abbey et al. demonstrated that even first-trimester CO exposure at environmentally relevant concentrations produces measurable perturbations in maternal and fetal hemodynamics, [5] while Tuoni et al. (2023) described the cascade of neonatal complications arising from gestational CO intoxication. [3]

The female reproductive system is particularly susceptible to hypoxic injury and oxidative stress. The uterus, as the central organ of reproductive physiology, depends critically on adequate oxygen delivery, stable microcirculatory function, and regulated cellular proliferation within both the endometrium and myometrium. [4] Recent research has established that hypoxia-inducible factor 1-alpha (HIF-1α) is a key molecular mediator of the uterine response to oxygen deficiency: under physiological conditions, transient endometrial hypoxia drives cyclic tissue regeneration, whereas sustained or pathological hypoxia promotes aberrant remodelling and glandular atrophy. [12] A 2024 review by Chen et al. comprehensively documented how dysregulation of the HIF-1α pathway in the endometrium contributes to a spectrum of pathological conditions, reinforcing the concept that uterine tissue is highly sensitive to changes in oxygen availability. [12] Oxidative stress in the reproductive tract is similarly consequential: Vornic et al. (2024) demonstrated associations between elevated oxidative stress biomarkers and placental pathology, [9] while Palmerini et al. (2023) showed that morphological and redox alterations in the PCOS uterus are intimately linked to oxidative imbalance. [8]

Despite these advances, the direct, concentration-dependent effects of chronic CO exposure on uterine histoarchitecture - specifically endometrial thickness and glandular density - have not been systematically investigated. Understanding the morphological consequences of graded CO exposure in the uterus is essential for characterising the reproductive toxicology of this ubiquitous pollutant and for developing evidence-based occupational and environmental health standards. The present study was designed to address this gap using a controlled four-group experimental inhalation model with quantitative morphometric analysis.

2. Materials and Methods

2.1. Animals and Housing

The study was conducted on 40 female Wistar rats (body weight 180–220 g; age 8–10 weeks), sourced from a single certified breeding facility and acclimatized for one week prior to study initiation. All animals were maintained under standardised laboratory conditions: ambient temperature 22–24 ℃, relative humidity 50–60%, and a 12-hour light/dark cycle with ad libitum access to standard pelleted rodent chow (protein 18%, fat 5%, carbohydrate 57%) and drinking water throughout the study period. Animals were housed in groups of five per cage during acclimatisation and individually during CO exposure to ensure precise dosimetry.

2.2. Ethical Statement

All experimental procedures were approved by the Institutional Animal Ethics Committee and conducted in strict accordance with international guidelines for the care and use of laboratory animals (Guide for the Care and Use of Laboratory Animals, 8th edition, National Research Council, 2011). All efforts were made to minimise animal suffering and to use the minimum number of animals consistent with statistical power requirements.

2.3. Experimental Design and CO Exposure

Animals were randomly allocated to four groups (n = 10 each) using a computer-generated random number sequence: Group I (Control) - ambient air, no CO exposure; Group II (CO-50) - continuous exposure to 50 ppm CO; Group III (CO-100) - continuous exposure to 100 ppm CO; Group IV (CO-200) - continuous exposure to 200 ppm CO. CO exposure was conducted for 4 consecutive weeks (28 days) in a purpose-built inhalation chamber (volume 200 L; stainless steel construction) with continuous CO concentration monitoring using a calibrated electrochemical sensor (accuracy ±2%; calibrated daily against certified reference gas). Chamber design incorporated active air exchange (15 air changes/hour) to ensure uniform CO distribution and prevent accumulation of CO_2, moisture, or other combustion by-products. Temperature, humidity, and O_2 concentration within the chamber were continuously monitored. Control animals were housed in an identical chamber supplied with filtered ambient air.

2.4. Tissue Collection and Histological Processing

At the end of the 28-day exposure period, animals were deeply anaesthetised with ketamine/xylazine (80/10 mg/kg, i.p.) and euthanised by exsanguination. The uterine horns were surgically excised, rinsed in cold physiological saline, and immediately fixed in 10% neutral-buffered formalin. Tissue processing followed the standardised histological protocol detailed in Table 1.

2.5. Morphometric Analysis

Histological sections were examined under a calibrated light microscope (magnification ×40–×400) equipped with a calibrated digital imaging system (Leica DM2500 with Leica Application Suite software). Endometrial thickness (μm) was measured as the perpendicular distance from the luminal epithelial surface to the inner myometrial border in five

randomly selected, non-overlapping fields per section using ImageJ image analysis software (NIH, Bethesda, MD, USA; version 1.54). Uterine gland count was performed by counting all glandular profiles visible in a standard field area (1 mm^2) in five non-overlapping fields per section. All measurements were performed by a single investigator blinded to group allocation, and mean values per animal were calculated for statistical analysis. The scale bar was calibrated for each objective magnification using a stage micrometer.

2.6. Statistical Analysis

Data are expressed as mean ± standard deviation (SD). Group differences were assessed using one-way ANOVA followed by Tukey's Honest Significant Difference (HSD) post hoc test for all pairwise comparisons. The Tukey HSD test was selected to control the familywise error rate across multiple comparisons. Effect size was quantified using the eta-squared (η^2) statistic, where $\eta^2 \geq 0.14$ indicates a large effect. Linear dose–response relationships were quantified by Pearson regression with R^2 and slope calculation. A p-value of < 0.05 was considered statistically significant. All analyses were performed using IBM SPSS Statistics version 26.0.

Table 1. Histological tissue processing protocol

Procedure	Reagent / Equipment	Duration / Notes
Fixation	10% neutral-buffered formalin	24 h
Dehydration	Graded ethanol (70%, 80%, 90%, 95%, 100%)	12 h total
Clearing	Xylene (2 changes)	2 h
Paraffin embedding	Paraffin wax (60 ℃ melting point)	3 h
Sectioning	Rotary microtome (Leica RM2255)	5 μm serial sections
Staining	Hematoxylin & Eosin (H&E)	Standard Mayer protocol
Coverslipping	DPX mountant	Permanent preparation

Table 2. Morphometric parameters by CO exposure group (Mean ± SD; n = 10/group)

Parameter	Control (0 ppm) n = 10	CO-50 (50 ppm) n = 10	CO-100 (100 ppm) n = 10	CO-200 (200 ppm) n = 10
Endometrial thickness, μm (Mean ± SD)	420 ± 18	395 ± 16	340 ± 21	285 ± 19
Change vs. control (%)	Ref.	−6.0%	−19.0%*	−32.1%**
Uterine gland count, per mm^2 (Mean ± SD)	28.0 ± 2.1	24.0 ± 1.9	19.0 ± 2.3	14.0 ± 1.8
Change vs. control (%)	Ref.	−14.3%*	−32.1%**	−50.0%**
p vs. control (Tukey HSD)	-	$p < 0.05$	$p < 0.001$	$p < 0.001$

*ET: endometrial thickness. GC: gland count. * $p < 0.05$ vs. control; ** $p < 0.001$ vs. control (Tukey HSD).*
% change expressed relative to control group mean.

Table 3. One-way ANOVA summary statistics for morphometric parameters

Parameter	F-statistic	df (between/within)	p-value (ANOVA)	η^2 (effect size)
Endometrial thickness (μm)	47.3	3 / 36	< 0.001	0.798
Uterine gland count (per mm^2)	51.6	3 / 36	< 0.001	0.812

df: degrees of freedom. η^2: eta-squared effect size. $\eta^2 \geq 0.14$ denotes large effect (Cohen, 1988).

Table 4. Tukey's HSD post hoc pairwise comparisons

Comparison	ET Mean Difference (μm)	ET p-value	GC Mean Difference (/mm^2)	GC p-value	Sig.
Control vs. CO-50	25	0.034	4.0	0.042	*
Control vs. CO-100	80	< 0.001	9.0	< 0.001	***
Control vs. CO-200	135	< 0.001	14.0	< 0.001	***
CO-50 vs. CO-100	55	< 0.001	5.0	< 0.001	***
CO-50 vs. CO-200	110	< 0.001	10.0	< 0.001	***
CO-100 vs. CO-200	55	< 0.001	5.0	0.002	**

*ET: endometrial thickness. GC: uterine gland count. * $p < 0.05$; ** $p < 0.01$; *** $p < 0.001$.*

3. Results

3.1. Overall Morphometric Findings

Chronic CO exposure produced significant, progressive, and concentration-dependent structural changes in uterine tissues across all experimental groups. One-way ANOVA confirmed statistically significant between-group differences for both morphometric parameters (Table 2 and Table 3). The large η^2 values (0.798 for endometrial thickness; 0.812 for gland count) indicate that CO exposure concentration accounted for approximately 80% of the total variance in both outcomes. All pairwise post hoc comparisons are detailed in Table 4.

3.2. Endometrial Thickness

In the control group, the endometrium displayed well-organised architecture with intact surface epithelium, abundant uterine glands, and normal lamina propria, with a mean endometrial thickness of 420 ± 18 µm. Exposure to 50 ppm CO produced a modest but statistically significant reduction to 395 ± 16 µm (−6.0%; $p < 0.05$ vs. control), consistent with early subclinical adaptive changes. At 100 ppm, thickness declined to 340 ± 21 µm (−19.0%; $p < 0.001$), indicating the onset of established structural disruption attributable to sustained tissue hypoxia and oxidative stress. At 200 ppm, endometrial thickness was reduced to 285 ± 19 µm - a 32.1% decrease relative to controls - reflecting pronounced mucosal atrophy and significant suppression of endometrial proliferative activity. Figures 1A and 1B provide graphical representations of the between-group comparisons. The dose–response relationship was strongly linear (Pearson $R^2 = 0.987$; slope = −0.68 µm/ppm; $p < 0.001$; Figure 2A).

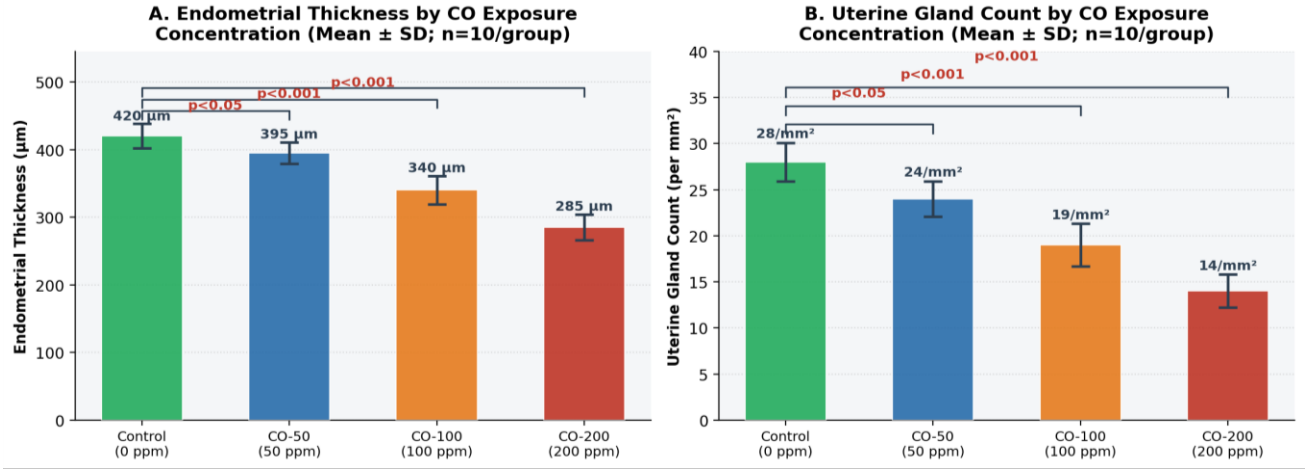

Figure 1. Dose-Dependent Morphometric Changes in Uterine Tissue Following Chronic CO Exposure (4-Week Inhalation Study; n = 10/group). A: Endometrial thickness (µm); B: Uterine gland count (per mm²). Bars represent Mean ± SD. Significance vs. control indicated above bars (Tukey HSD: * $p < 0.05$, *** $p < 0.001$). Color coding: green = control; blue = 50 ppm; orange = 100 ppm; red = 200 ppm

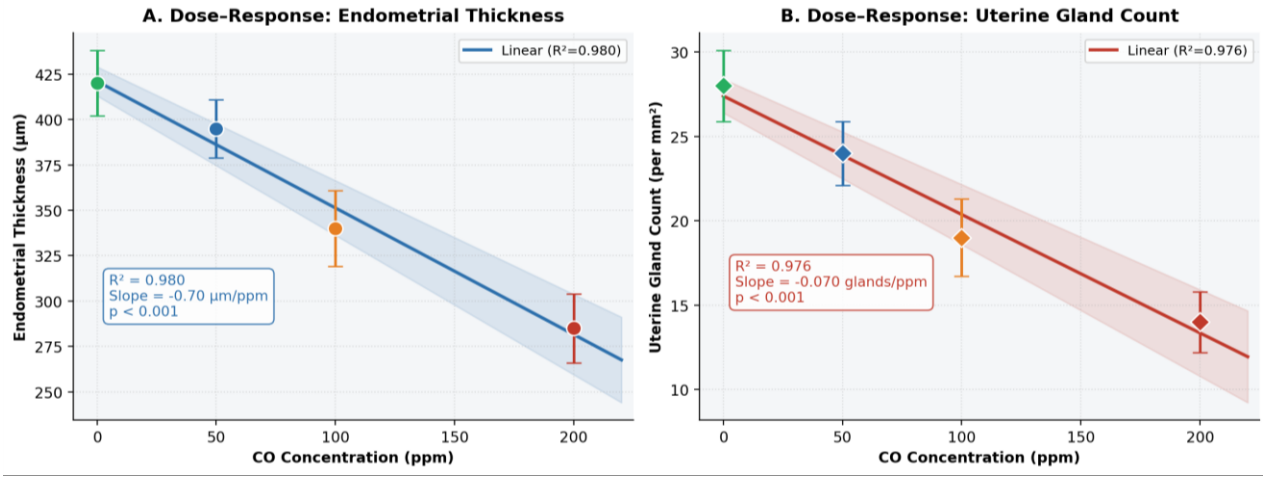

Figure 2. Linear Dose–Response Relationships Between CO Exposure Concentration and Uterine Morphometric Parameters. A: Endometrial thickness; B: Uterine gland count. Data points: individual group means ± SD color-coded by group. Shaded band: 95% confidence interval of the regression line. R^2 values and slope coefficients inset

3.3. Uterine Gland Count

The number of uterine glands per standard field also declined progressively with increasing CO concentration. The control group displayed 28.0 ±2.1 glandular profiles per mm ², consistent with normal endometrial histoarchitecture. Exposure to 50 ppm reduced gland count to 24.0 ± 1.9/mm ² (−14.3%; $p < 0.05$), indicating early impairment of glandular homeostasis. At 100 ppm, gland number decreased to 19.0 ± 2.3/mm² (−32.1%; $p < 0.001$), reflecting deeper morphological disruption and probable reduction in endometrial functional activity. At 200 ppm, gland count fell to a minimum of 14.0 ± 1.8/mm ² - a 50.0% reduction compared with controls ($p < 0.001$) - indicating marked depletion of the glandular compartment with likely consequences for endometrial secretory function and implantation capacity. The dose–response relationship was highly linear ($R^2 = 0.998$; slope = −0.070 glands·mm^{-2}·ppm^{-1}; $p < 0.001$; Figure 2B).

3.4. Statistical Distribution Analysis

Box-plot analysis with individual data points confirmed the consistency of morphometric measurements within each group, with low intragroup variability (Figure 3). All groups demonstrated compact interquartile distributions without influential outliers, confirming the reliability of the blinded measurement protocol. The progressive downward shift of the entire distribution - not merely the group mean - at each successive CO concentration confirms that the dose-dependent effect is consistent across all individual animals rather than driven by outlier observations.

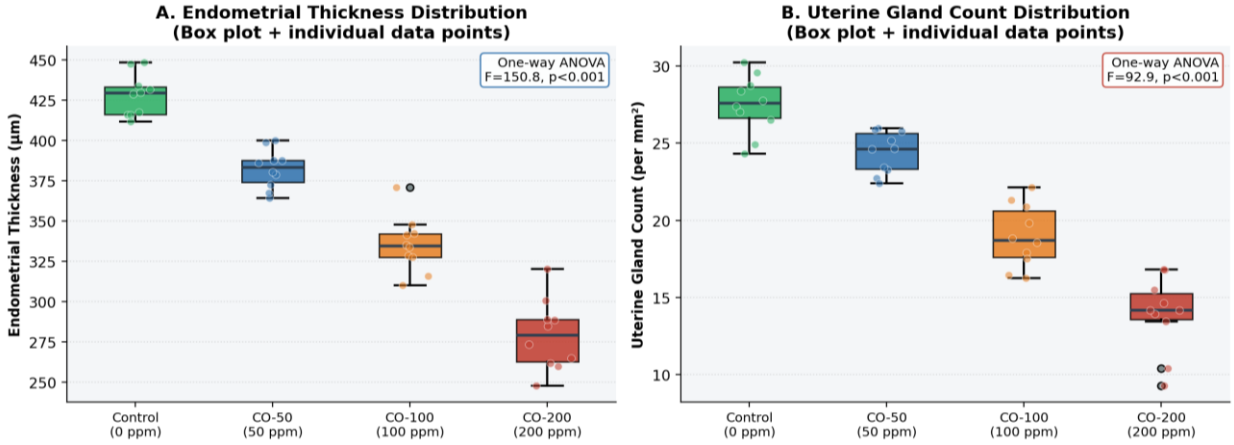

Figure 3. One-Way ANOVA: Distribution of Morphometric Parameters Across Groups (n = 10/group). A: Endometrial thickness; B: Uterine gland count. Box plots show median, interquartile range, and whiskers (1.5 × IQR). Individual data points overlaid (jitter applied). One-way ANOVA F-statistic and p-value inset

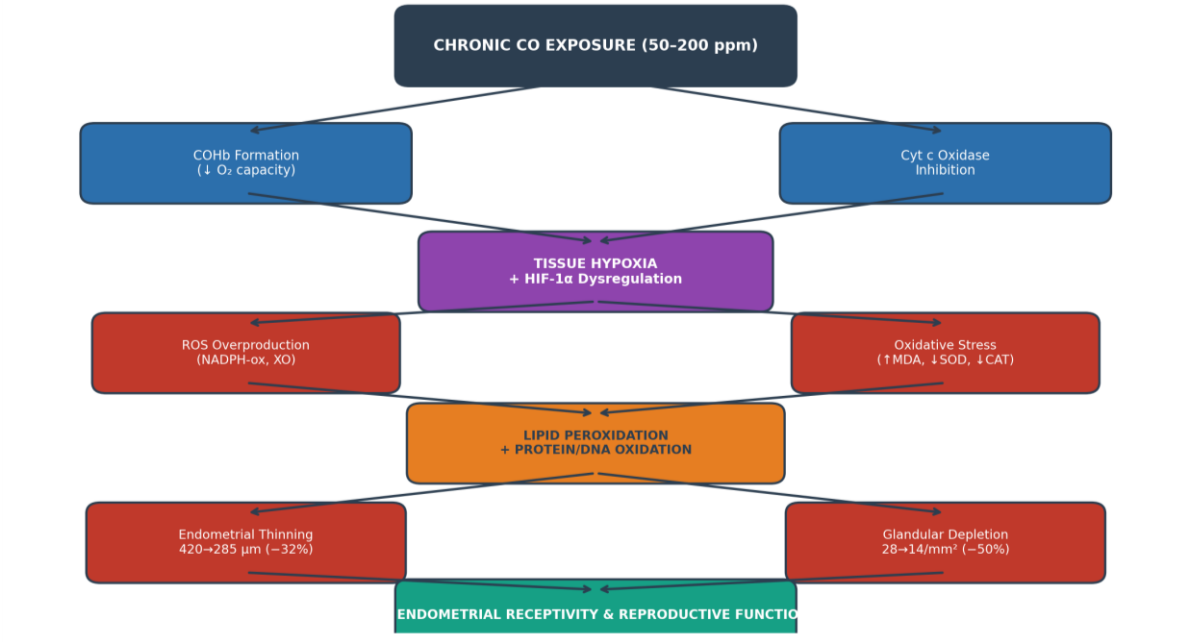

Figure 4. Proposed Mechanistic Pathway of CO-Induced Uterine Morphological Injury. COHb: carboxyhemoglobin; ROS: reactive oxygen species; MDA: malondialdehyde; SOD: superoxide dismutase; CAT: catalase; HIF-1α: hypoxia-inducible factor 1-alpha; XO: xanthine oxidase. Arrows indicate pathogenic cascade; outlined boxes represent quantified outcomes from the present study

4. Discussion

The present study provides experimental evidence that chronic CO exposure induces significant, concentration-dependent morphological deterioration of the uterus in female Wistar rats, as evidenced by progressive endometrial thinning and glandular depletion across the three tested concentrations. The clear linear dose–response relationships ($R^2 = 0.987$ for endometrial thickness; $R^2 = 0.998$ for gland count) and the large effect sizes ($\eta^2 > 0.79$) confirm the robustness and biological consistency of these findings. The proposed mechanistic pathway integrating CO-induced hypoxia and oxidative stress is illustrated in Figure 4.

The dose-dependent reduction in endometrial thickness is consistent with the well-established pathophysiological consequences of tissue hypoxia in the female reproductive tract. CO-induced COHb formation reduces blood oxygen-carrying capacity, [3] while simultaneous cytochrome c oxidase inhibition impairs mitochondrial respiration at the cellular level - a dual mechanism of functional hypoxia generation that is particularly injurious to the metabolically active endometrium. [14] As documented by Chen et al. (2024), sustained activation of the HIF-1α pathway under pathological hypoxic conditions leads to aberrant endometrial remodelling rather than the regulated regeneration seen under physiological conditions. [12] Our morphometric data are consistent with this concept: the progressive endometrial thinning across CO concentrations suggests chronic hypoxia suppresses normal proliferative activity and impairs the regenerative capacity of endometrial epithelium. The 50 ppm group, while showing statistically significant changes, exhibited a modest effect (−6.0% thickness reduction), possibly representing a compensated adaptive response below the threshold of irreversible injury. In contrast, the 200 ppm group - showing −32.1% endometrial thinning and −50.0% glandular depletion - likely reflects a transition toward structural changes with lasting functional consequences.

The concurrent reduction in uterine gland number is particularly significant from a reproductive perspective. Uterine glands are essential for the synthesis and secretion of histotroph - the nutritive fluid supporting early embryo development and the pre-implantation environment. Glandular atrophy and reduced glandular density, as observed at 100 and 200 ppm in our study, would be expected to compromise endometrial receptivity and implantation capacity. These findings are broadly consistent with Palmerini et al. (2023), who demonstrated morphological and redox alterations in the PCOS uterus including glandular disruption linked to oxidative imbalance, [8] and with Karakus et al. (2023), who reported dose-dependent histological and hormonal alterations in the reproductive system of rats exposed to the pesticide thiamethoxam, with glandular density sensitive to oxidative injury. [15] The 50% glandular depletion at 200 ppm CO observed in our study is a particularly striking finding that, if translatable to the human context, would predict substantially impaired endometrial secretory function during the implantation window.

The mechanistic link between CO exposure and oxidative stress underlying our histological findings has been increasingly characterised in recent literature. Angelova et al. (2023) demonstrated that CO neurotoxicity involves ROS production from three distinct cellular sources - mitochondria, NADPH oxidase, and the xanthine oxidase system - all of which would be expected to be operative in uterine tissue under CO exposure conditions. [14] López et al. (2008) provided direct experimental evidence that prenatal chronic mild CO exposure generates cochlear oxidative stress in a dose-dependent manner, confirming the capacity of CO to amplify oxidative injury beyond the hemoglobin-binding mechanism. [7] Our histomorphological findings - progressive structural changes at 100 and 200 ppm - are consistent with this cascade of oxidative injury superimposed upon hypoxic suppression of proliferative signalling.

The dose-response relationship established in our study carries direct public health implications. Epidemiological studies have linked chronic CO exposure to adverse reproductive outcomes including intrauterine growth restriction and preterm birth at concentrations well below 50 ppm in the context of maternal smoking and environmental exposure. [8] The WHO air quality guidelines and the US OSHA permissible exposure limit for CO in occupational settings (35–50 ppm as time-weighted average) are based primarily on cardiovascular and neurological endpoints; our data suggest that reproductive endpoints - specifically uterine morphological integrity - may be sensitive at similar or lower concentrations. [4,5] CO accumulation in the fetal compartment exceeds maternal levels due to the higher CO affinity of fetal haemoglobin, [9] potentially amplifying reproductive consequences in pregnant women.

Several limitations warrant acknowledgment. First, the study did not include direct biochemical measurements of oxidative stress markers - malondialdehyde, superoxide dismutase activity, catalase activity - which would have provided molecular corroboration of the histological findings and the proposed mechanistic pathway (Figure 4). This represents a priority for follow-up investigation. Second, hormonal status and estrous cycle phase were not systematically controlled across experimental groups, which may introduce biological variability in endometrial measurements; randomisation partially mitigates this concern. Third, the continuous inhalation exposure protocol may not fully replicate intermittent real-world environmental scenarios. Fourth, the study is limited to morphometric endpoints; future studies should incorporate immunohistochemical markers of cellular proliferation (Ki-67), apoptosis (caspase -3), and hypoxia signalling (HIF-1α) to comprehensively characterise the molecular mechanisms. Strengths of this study include the controlled four-group dose-escalation design, blinded morphometric assessment, calibrated inhalation chamber with real-time CO monitoring, large effect sizes, strong linear dose–response relationships, and rigorous statistical analysis including post hoc testing and effect size quantification.

5. Conclusions

Chronic CO exposure induces significant, dose-dependent histological and morphometric changes in the uterus of female Wistar rats, including progressive endometrial thinning (−6.0%, −19.0%, and −32.1% at 50, 100, and 200 ppm respectively; all $p < 0.05$ vs. control) and substantial reduction in uterine gland number (−14.3%, −32.1%, and −50.0% respectively; all $p < 0.05$ vs. control). Strong linear dose–response relationships were confirmed for both parameters ($R^2 = 0.987$ and 0.998). The large effect sizes ($\eta^2 > 0.79$) confirm that CO concentration accounts for the majority of morphometric variability. These changes are consistent with the combined pathological effects of COHb-mediated tissue hypoxia, cytochrome c oxidase inhibition, HIF-1α pathway dysregulation, and ROS-driven oxidative injury on the proliferative and secretory functions of the endometrium.

From a public health perspective, these findings are relevant to occupational and environmental settings involving chronic low-to-moderate CO exposure - including vehicle traffic, mining, and indoor combustion - where women of reproductive age represent a particularly vulnerable subpopulation. Current occupational CO exposure limits, designed primarily to protect against cardiovascular and neurological endpoints, may not adequately safeguard reproductive tract integrity. Regulatory bodies and occupational health authorities should consider incorporating uterine morphological and reproductive endpoints into CO risk assessment frameworks.

Future investigations should: (1) incorporate biochemical oxidative stress markers (MDA, SOD, CAT) alongside morphometry to provide molecular corroboration; (2) include immunohistochemical analysis of HIF-1α, Ki-67, and caspase-3 expression to characterise proliferative, apoptotic, and hypoxic signalling responses; (3) assess hormonal profiles (oestradiol, progesterone, FSH, LH) to determine whether CO-induced morphological changes are partly mediated through hypothalamic-pituitary-ovarian axis disruption; (4) evaluate reversibility of morphometric changes following cessation of CO exposure; and (5) apply intermittent exposure protocols that more closely replicate occupational and environmental scenarios.

Ethics Approval

Institutional Animal Ethics Committee, Protocol No. [number], [date]. All procedures conducted per the Guide for the Care and Use of Laboratory Animals, 8th edition (NRC, 2011).

Conflicts of Interest

None declared.

Funding

Institutional resources only. No external funding received.

REFERENCES

[1] Asadi B. et al. Carbon monoxide refines ovarian structure changes and attenuates oxidative stress via modulating of heme oxygenase system in a rat model of polycystic ovary syndrome: an experimental study. International Journal of Reproductive Biomedicine. 2024; 22(8): 627.

[2] Balbo L.C. et al. Reproductive tissue toxicity of deoxynivalenol and α-zearalenol alone or in combination: insights from a porcine explant model. Toxicology and Applied Pharmacology. 2025; 117605.

[3] Tuoni C., Nuzzi G., Scaramuzzo R.T., Fiori S., Filippi L. Neonatal hypoxic-ischemic encephalopathy after acute carbon monoxide intoxication during pregnancy: a case report and brief review of the literature. Frontiers in Pediatrics. 2023; 11: 1264855.

[4] Itziou A. et al. Environmental pollution and oxidative stress: health effects during pregnancy. Applied Sciences. 2024; 14(21): 9884.

[5] Abbey M. et al. Medical biomonitoring of maternal and fetal exposure to carbon monoxide and its modification by demographic and obstetric characteristics. Nigerian Medical Journal. 2024; 64(6): 744–758.

[6] Li Y. et al. Baicalein improves the symptoms of polycystic ovary syndrome by mitigating oxidative stress and ferroptosis in the ovary and gravid placenta. Phytomedicine. 2024; 128: 155423.

[7] Lopez I.A. et al. Oxidative stress and the deleterious consequences to the rat cochlea after prenatal chronic mild exposure to carbon monoxide in air. Neuroscience. 2008; 151(3): 854–867.

[8] Palmerini M.G. et al. Modulating morphological and redox/glycative alterations in the PCOS uterus: effects of carnitines in PCOS mice. Biomedicines. 2023; 11(2): 374.

[9] Vornic I. et al. Oxidative stress and placental pathogenesis: a contemporary overview of potential biomarkers and emerging therapeutics. International Journal of Molecular Sciences. 2024; 25(22): 12195.

[10] Zhang J. et al. Bushen Jianpi Tiaoxue Decoction (BJTD) ameliorates oxidative stress and apoptosis induced by uterus ageing through activation of the SIRT1/NRF2 pathway. Phytomedicine. 2025; 136: 156288.

[11] Mahan V.L. Heme oxygenase/carbon monoxide system affects the placenta and preeclampsia. Medical Gas Research. 2025; 15(2): 276–287.

[12] Chen X. et al. Hypoxia and the endometrium: an indispensable role for HIF-1α as therapeutic strategies. Redox Biology. 2024. doi: 10.1016/j.redox.2024.103431

[13] Letafati A. et al. Emerging paradigms: unmasking the role of

oxidative stress in HPV-induced carcinogenesis. Infectious Agents and Cancer. 2024; 19(1): 30.

[14] Angelova P.R., Myers I., Abramov A.Y. Carbon monoxide neurotoxicity is triggered by oxidative stress induced by ROS production from three distinct cellular sources. Redox Biology. 2023; 60: 102598.

[15] Karakus A. et al. Induction of apoptosis, oxidative stress, hormonal, and histological alterations in the reproductive system of thiamethoxam-exposed female rats. Environmental Science and Pollution Research. 2023; 30: 78543–78558.

Copyright © 2026 The Author(s). Published by Scientific & Academic Publishing
This work is licensed under the Creative Commons Attribution International License (CC BY). http://creativecommons.org/licenses/by/4.0/